General Solution for Tidal Behavior in Confined and Semiconfined Aquifers Considering Skin and Wellbore Storage Effects

Xuhua Gao[1], Kozo Sato[1,2], Roland N. Horne[1]

[1]Stanford University, Stanford, CA 94305, USA
[2]The University of Tokyo, 7-3-1 Hongo Bunkyo-ku Tokyo 113-8656, Japan

Key Points:

- Skin and wellbore storage effects have significant impacts on tidal analysis results and are thus included in tidal models.
- The new models are established for both confined and semiconfined aquifers and demonstrated with real-world examples.
- The existence of a negative skin can cause a phase advance between the tidal response and the theoretical tide.

Corresponding author: Xuhua Gao, xuhuag@stanford.edu

Abstract

Tidal analysis provides a cost-effective way of estimating aquifer properties. Tidal response models that link aquifer properties with tidal signal characteristics, such as phase and amplitude, have been established in previous studies, but none of the previous models incorporate the skin effect. It is found in this study that the skin effect and the wellbore storage effect can have significant influence on the results of tidal analysis and should be included in tidal response models. New models are proposed with skin and wellbore storage effects fully incorporated, so that aquifer information can be assessed more accurately based on tidal analysis. The models can be applied to confined aquifers with only horizontal flow or semiconfined aquifers with both horizontal flow and vertical flow. For confined aquifers, the new model indicates that positive skin leads to larger phase lag between the tidal response the the theoretical tide, and negative skin can reduce the phase lag or even cause a phase advance. For semiconfined aquifers, both the skin effect and the vertical flow affect the phase difference between the tidal response and the theoretical tide, and with the proposed model, contribution from these two sources can be separated and analyzed independently, making it feasible to evaluate semiconfined aquifer properties considering both factors. Increasing wellbore storage causes larger phase lag or smaller phase advance for both types of aquifers. Real-world examples for confined and semiconfined aquifers are analyzed respectively to demonstrate practical applications of the proposed models.

1 Introduction

The Earth tides, which are caused by the gravitational forces exerted on the Earth by celestial bodies including the Moon and the Sun, result in aquifer deformations, and the response of the aquifer can be reflected by the change in wellbore pressure in a closed well or the fluid flow into and out of the wellbore in an open well. The effects of Earth tide on confined and semiconfined aquifers have long been studied by hydrologists for the purpose of extracting useful aquifer information from cyclic tidal responses. The comparison between actual tidal responses and the theoretical tides can reveal aquifer properties such as transmissivity and compressibility. Typically, tidal data can be analyzed from two perspectives - amplitude and phase. The ratio of tidal data amplitude to theoretical tide amplitude is associated with poroelastic properties of the formation including Skempton's coefficient, bulk modulus, Poisson's ratio, etc. (Van der Kamp & Gale, 1983; Sato, 2006; Burbey, 2010; Bredehoeft, 1967; Arditty et al., 1978; Sato & Horne, 2018). Aquifer flow properties, such as permeability, are more closely related with the phase difference between tidal data and the theoretical tide. Cooper et al. (1967) found that water level changes in open wells due to harmonic disturbances have the same frequency as the disturbance, although phases and amplitudes of the water level response are generally different from those of the disturbance, depending on transmissivity and storage coefficient of the aquifer and period of the disturbance. Hsieh et al. (1987) applied the diffusion equation to model the phase lag between the tidal response induced by the Earth tide and the theoretical tide as a function of transmissivity and storativity of the aquifer, wellbore radius, and period of the Earth tide, assuming that the formation is confined, laterally extensive, homogeneous and isotropic. According to Hsieh et al. (1987), there is always a phase lag under those assumptions because time is needed for the fluid in the aquifer to respond to tidal forces and flow into or out of the well. Other researchers suggested that phase advance, with measured tidal response leading theoretical tides, could exist under some different scenarios. For example, in a composite system, when a compressible aquifer is surrounded by more rigid aquifers, tidal responses measured in the well tapping the compressible aquifer can lead the theoretical tide due to the tidal strain differentiation between adjoining aquifers (Gieske & De Vries, 1985). Maas and De Lange (1987) explained a similar phenomenon of phase advance using the principle of superposition. Another case in which a phase advance can happen is when the aquifer is not perfectly confined (i.e. semiconfined) and there is a vertical leakage from the target aquifer to the overlaying aquifer. Allègre et al. (2016) applied a vertical flow model to explain the phase advance and infer permeability from water level variations without considering the

horizontal flow. Wang et al. (2018) considered both the horizontal flow and the vertical leakage and extended Hsieh's model (Hsieh et al., 1987) using the specific leakage, which is defined as the ratio of hydraulic conductivity to thickness of the leaking aquitard. Based on the model presented by Wang et al. (2018), when aquifer transmissivity and storativity are known, the magnitude of the vertical leakage can be estimated.

However, none of the models discussed above considered the skin effect, and the wellbore storage effect is not explicitly incorporated, even though the flow transient in the wellbore can be strongly affected by the wellbore storage effect and the skin effect. Wellbore storage effect is commonly caused by fluid expansion or changing liquid level and is characterized by the wellbore storage coefficient. The skin effect can be due to a zone surrounding the well that is penetrated by cement or mud filtrate generated during the drilling or completion processes, and can cause significant permeability change in the affected zone. It is found in this study that the wellbore storage coefficient and the skin factor are important parameters influencing the results of tidal analysis, and should be incorporated in tidal response models to improve the accuracy and reliability of the estimation of aquifer properties based on tidal analysis. Therefore, new tidal response models for both confined aquifers and semiconfined aquifers with skin effect and wellbore storage effect taken into consideration are proposed in this study. Analytical solutions and applications of the models are illustrated in detail, and the change in tidal analysis results due to various skin factors are explained and demonstrated with real-world examples on the basis of previous work by Hsieh et al. (1987) and Wang et al. (2018) for confined aquifers and semiconfined aquifers respectively.

Purposes and potential applications of this study include:

1. Incorporation of wellbore storage and skin effect into tidal analysis and its application, considering both confined and semiconfined aquifer.
2. If the aquifer transmissivity is known, wellbore storage or skin can be quantified using the Earth tide analysis without the need for well flow test or pumping test. Determination of wellbore storage and skin is important for pressure transient analysis and wellbore and aquifer property estimation. The conventional way of evaluating wellbore storage and skin involves interpretation of well test data or pumping test data (Gringarten et al., 1979; Ramey Jr, 1970; Cinco-Ley & Samaniego, 1977). However, when well test data or pumping test data are not available (e.g. when the well is closed and static), conventional methods cannot be applied. As proposed in this study, an alternative method to determine wellbore storage or skin takes advantage of the Earth tide analysis. The Earth tide effect influences pressures in closed wells or water levels in open wells regardless of whether the well is active or not. By modelling the pressure change or fluid flow induced by tidal forces, we can estimate wellbore storage or skin based on tidal responses measured at the wellbore.
3. For a confined aquifer, if the wellbore storage coefficient and the skin factor are known, the aquifer transmissivity can be estimated based on tidal analysis. The main difference between our method and the method originally proposed by Hsieh et al. (1987) is that the skin effect is fully considered in our model.
4. For a semiconfined aquifer, if the wellbore storage coefficient, the skin factor, and the aquifer transmissivity are known, the magnitude of vertical leakage can be evaluated from tidal analysis. The original model for tidal responses in semiconfined aquifers was established by Wang et al. (2018), and the new model in this study considers the skin effect and adds the skin factor as an input parameter.
5. Explanation of the phenomena of phase advance from the perspective of enhanced permeability characterized by the negative skin. It is found that both negative skin and vertical leakage can lead to a phase advance. With the model proposed in this paper, it is possible to separate these two effects and evaluate skin independently even when vertical leakage exists.

Table 1. Major tidal constituents

Doodson's number	Name	Freq.(cpd)	Origin	Amplitude(m)
Low frequency tides				
0 1 0-1 0 0	M_m	0.0363	Lunar elliptic	-0.03518
0 2 0 0 0 0	M_f	0.0732	Lunar declinational	-0.06663
Diurnal tides				
1-1 0 0 0 0	O_1	0.9295	Lunar principal	-0.26221
1 1-2 0 0 0	P_1	0.9973	Solar principal	-0.12203
1 1 0 0 0 0	K_1	1.0027	Luni-solar declinational	0.36878
Semidiurnal tides				
2-1 0 1 0 0	N_2	1.8961	Lunar major elliptic of M_2	0.12099
2 0 0 0 0 0	M_2	1.9324	Lunar principal	0.63192
2 2-2 0 0 0	S_2	2.0000	Solar principal	0.29400

2 Theory

2.1 Tidal forces

The Moon and the Sun apply gravitational forces on the Earth, causing deformation of the aquifer and pressure change or fluid flow at the wellbore. The tidal waves are composed of various tidal constituents from a wide spectrum. Each tidal constituent is a sinusoidal function of time with an amplitude determined from the equilibrium tide and a period resulting from the cyclic motion of the Moon, the Sun and the Earth (Melchior, 1983; Hicks & Szabados, 2006; Bartels, 1957). The theoretical tidal potential at a location with east longitude ψ and colatitude θ can be expressed as:

$$\eta(\theta,\psi,t) = \sum_i H_i(\theta,\psi)\cos(\omega_i t + \chi_i + \delta_i(\theta,\psi)) \tag{1}$$

where the subscript i corresponds to each harmonic tidal constituent. H is the amplitude, and ω is the tidal frequency. χ is an astronomical argument (Schwiderski, 1980). δ is the Greenwich phase with t being Greenwich time (GMT). Based on its tidal frequency, a tidal constituent can be categorized as a diurnal component, a semidiurnal component or a long-period component. Major tidal constituents and their amplitudes and frequencies are listed in Table 1 (Melchior, 1966; D. E. Cartwright & Tayler, 1971; D. Cartwright & Eden, 1973).

The observed tidal responses (e.g. water level or pressure variations) follow a form similar to Equation 1 with the same tidal constituents but different amplitudes H' and phases δ'.

$$\eta'(\theta,\psi,t) = \sum_i H'_i(\theta,\psi)\cos(\omega_i t + \chi_i + \delta'_i(\theta,\psi)) \tag{2}$$

Aquifer and well properties determine the amplitude ratio H'_i/H_i and the phase difference $\delta'_i - \delta_i$. The observed tidal response can be decomposed into different harmonic constituents using Fourier analysis, and the amplitude H'_i and phase δ_i for a specific constituent can be retrieved from the data. Theoretical amplitudes and phases are known, so H'_i/H_i and $\delta'_i - \delta_i$ can be obtained from the data. The models discussed in Section 2.2 and 2.3 relate aquifer and well properties to the amplitude ratio and the phase difference, considering the wellbore storage effect and the skin effect.

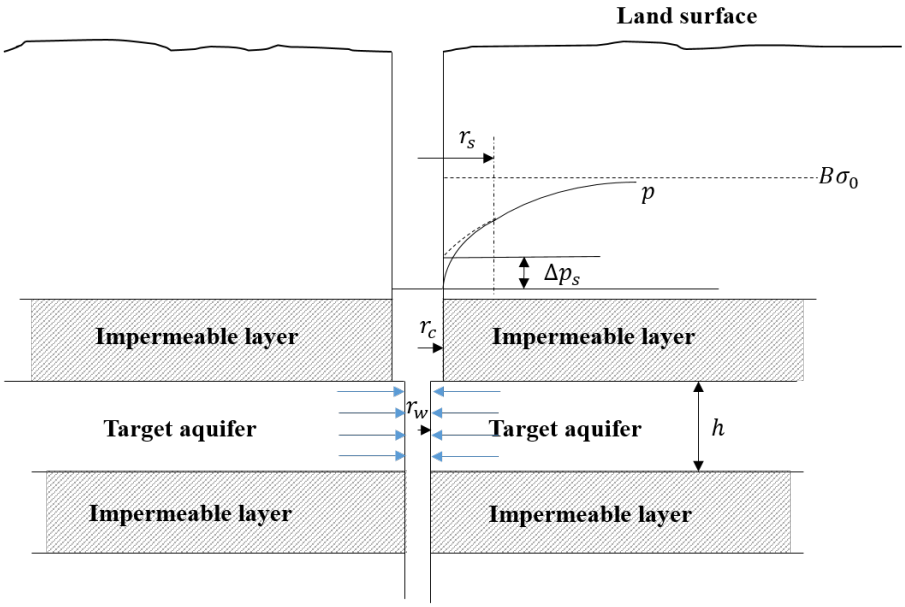

Figure 1. Confined aquifer system

2.2 Confined aquifer

When the aquifer is confined, vertical flow is prevented by impermeable layers both above and below the aquifer. A schematic of a confined aquifer system is shown in Figure 1. The well in Figure 1 is closed, and the target aquifer is penetrated by the well entirely. Tidal forces cause a cyclic pressure fluctuation at the wellbore. r_c and r_w are casing radius and wellbore radius respectively. h is the thickness of the target aquifer. The damaged zone that causes the skin effect has a radius of r_s, and the skin effect results in a pressure drop Δp_s at the wellbore. The skin factor can be defined as:

$$s = \frac{\Delta p_s}{(r\frac{\partial p}{\partial r})_{r=r_w}} \tag{3}$$

where p is the excess pressure in the aquifer above the initial baseline pressure.

It is assumed that outside the damaged zone the aquifer is isotropic, homogeneous and laterally extensive. The flow transient in a confined aquifer system (Figure 1) under the cubic tidal stress σ_t is governed by the following equation:

$$\frac{\partial^2 p}{\partial r^2} + \frac{1}{r}\frac{\partial p}{\partial r} = \frac{\phi\mu c_t}{k}\left(\frac{\partial p}{\partial t} - B\frac{\partial \sigma_t}{\partial t}\right) \tag{4}$$

where μ is the fluid viscosity. c_t is the total compressibility, and B is Skempton's coefficient. The outer boundary condition for the laterally extensive aquifer ($r = \infty$), as shown in Figure 1, can be expressed as:

$$p(\infty, t) = B\sigma_t(t) \tag{5}$$

The inner boundary conditions involving the skin effect and the wellbore storage effect are:

$$p_w = \left[p - s\left(r\frac{\partial p}{\partial r}\right)\right]_{r=r_w} \tag{6}$$

$$C\frac{dp_w}{dt} = \frac{2\pi kh}{\mu}\left(r\frac{\partial p}{\partial r}\right)_{r=r_w} \tag{7}$$

where p_w is the pressure measured inside the wellbore. s is the skin factor, and C is the wellbore storage coefficient. This system of equations can be simplified if we define:

$$\overline{p}(r,t) = p(r,t) - B\sigma_t(t) \tag{8}$$

Then the governing equation becomes:

$$\frac{\partial^2 \overline{p}}{\partial r^2} + \frac{1}{r}\frac{\partial \overline{p}}{\partial r} = \frac{\phi\mu c_t}{k}\frac{\partial \overline{p}}{\partial t} \tag{9}$$

and the boundary conditions become:

$$\overline{p}(\infty,t) = 0 \tag{10}$$

$$p_w = \left[\overline{p} - s\left(r\frac{\partial \overline{p}}{\partial r}\right)\right]_{r=r_w} + B\sigma_t \tag{11}$$

$$C\frac{dp_w}{dt} = \frac{2\pi kh}{\mu}\left(r\frac{\partial \overline{p}}{\partial r}\right)_{r=r_w} \tag{12}$$

From Equation 1, we know that the tidal stress that causes the pressure fluctuation is a cyclic function of time. As a result, tide-induced fluid pressure and wellbore pressure oscillations also follow a cyclic pattern.

$$\sigma_t(t) = \sigma_0(\omega)\exp(i\omega t) \tag{13}$$

$$\overline{p}(r,t) = p_0(r,\omega)\exp(i\omega t) \tag{14}$$

$$p_w(t) = p_{w0}(\omega)\exp(i\omega t) \tag{15}$$

where i is the imaginary unit. ω is the tidal frequency, and $\sigma_0(\omega)$, $p_0(r,\omega)$ and $p_{w0}(\omega)$ are complex amplitudes of the cubic tidal stress, fluid pressure and wellbore pressure fluctuations, respectively. By inserting Equations 13-15 into Equations 9-12, we can reduce the governing equation to an ordinary differential equation:

$$\frac{d^2 p_0}{dr^2} + \frac{1}{r}\frac{dp_0}{dr} = i\omega\frac{\phi\mu c_t}{k}p_0 \tag{16}$$

with the following boundary conditions:

$$p_0(\infty,\omega) = 0 \tag{17}$$

$$p_{w0} = \left[p_0 - s\left(r\frac{\partial p_0}{\partial r}\right)\right]_{r=r_w} + B\sigma_0 \tag{18}$$

$$i\omega C p_{w0} = \frac{2\pi kh}{\mu}\left(r\frac{\partial p_0}{\partial r}\right)_{r=r_w} \tag{19}$$

The general solution to Equation 16 is:

$$p_0(r,\omega) = A_1 I_0\left(r\sqrt{\frac{i\omega\phi\mu c_t}{k}}\right) + A_2 K_0\left(r\sqrt{\frac{i\omega\phi\mu c_t}{k}}\right) \tag{20}$$

where I_0 and K_0 are the zero-order modified Bessel function of the first and second kind respectively. The outer boundary condition gives that $A_1 = 0$. From the boundary condition, Equation 19, the constant A_2 can be obtained as:

$$\begin{aligned} A_2 &= -\frac{i\omega\mu C}{2\pi khr_w\sqrt{i\omega\phi\mu c_t/k}K_1(r_w\sqrt{i\omega\phi\mu c_t/k})}p_{w0} \\ &= -\frac{\alpha_D}{2S_D K_1(\alpha_D)}p_{w0} \end{aligned} \tag{21}$$

where α_D and S_D are defined as follows:

$$\alpha_D = r_w\sqrt{\frac{i\omega\phi\mu c_t}{k}} = \sqrt{\frac{2\pi i S_D}{T_D}} \tag{22}$$

$$S_D = \frac{\pi\phi c_t h r_w^2}{C} = \frac{1}{2C_D} \tag{23}$$

$$T_D = \frac{2\pi^2 kh}{C\mu\omega} = \frac{\pi\tau kh}{C\mu} \tag{24}$$

where C_D is the dimensionless wellbore storage coefficient and $\tau = 2\pi/\omega$ is the period of fluctuation. In this case, T_D and S_D can be comprehended as dimensionless transmissivity and storativity, and they are related with conventional aquifer transmissivity and storativity through the following equations:

$$\frac{T_D}{T} = \frac{\pi\tau}{C\rho g} \tag{25}$$

$$\frac{S_D}{S} = \frac{\pi r_w^2}{C\rho g} \tag{26}$$

where T is the conventional aquifer transmissivity ($T = \frac{kh}{\mu}\rho g$), which is defined as the product of hydraulic conductivity and aquifer thickness. S is the conventional aquifer storativity ($S = \phi c_t h\rho g$) and is the product of aquifer specific storage and thickness. ρ is water density, and g is the gravitational acceleration.

From the inner boundary condition, Equation 18, p_{w0} is obtained as:

$$p_{w0} = \left[1 + \frac{\alpha_D}{2S_D}\frac{K_0(\alpha_D)}{K_1(\alpha_D)} + \pi i\frac{s}{T_D}\right]^{-1} B\sigma_0 \tag{27}$$

We can see from Equation 27 that at the wellbore the pressure response to tidal forces is a function of not only aquifer storativity and transmissivity but wellbore storage coefficient and skin factor as well. As a result, the solution provides a way to estimate wellbore storage coefficient and skin factor from tidal analysis given aquifer storativity and transmissivity. On the other hand, if aquifer storativity and transmissivity are unknown, they can be inferred from tidal analysis under different wellbore storage and skin scenarios. Applications of the solution are discussed in more detail in Section 3.

The original partial differential equation can be solved with the Laplace transform as well. Numerical inversion of the solution in Laplace space provides the same result as Equation 27. Note that when the well is active with a flow rate other than zero, we can only use the Laplace transform method to solve this problem. Details about the solution obtained from Laplace transformation are included in the Appendix.

2.3 Semiconfined aquifer

The key difference between a semiconfined aquifer and a confined aquifer is the existence of vertical flow. In a semiconfined aquifer, there can be both horizontal flow and vertical flow. The configuration of semiconfined aquifer considered in this section is illustrated in Figure 2. The target aquifer is overlain by a permeable aquitard, and above the permeable aquitard is an unconfined aquifer. Such a classical leaky aquifer model was first studied by Hantush and Jacob (1955). Wang et al. (2018) investigated a similar system and estimated the magnitude of vertical leakage with tidal analysis. The solution proposed by Wang et al. (2018) is extended with the inclusion of skin effect in this study.

It is assumed that both the overlaying permeable aquitard and the target aquifer are laterally extensive, and that the permeable aquitard has negligible storage and is incompressible. The governing equation is similar to Equation 4 but with a term that accounts

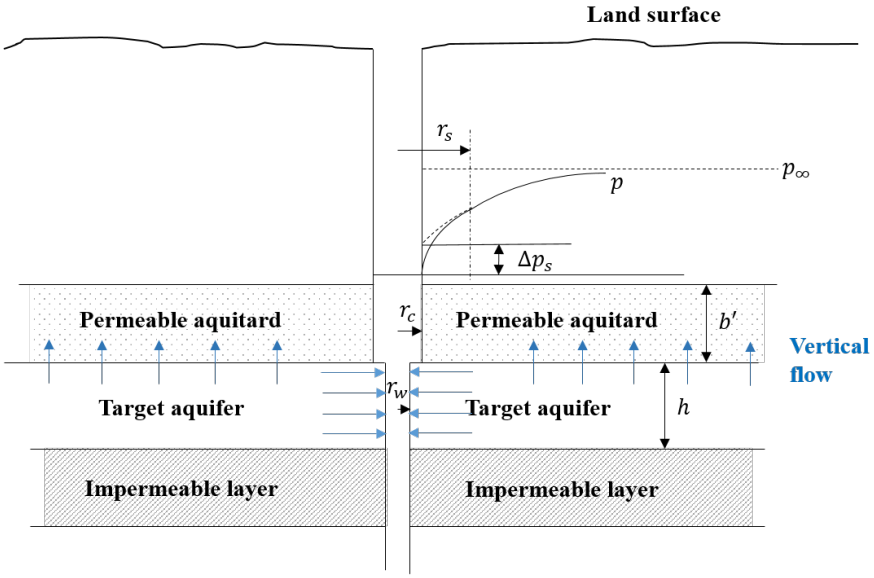

Figure 2. Semiconfined aquifer system

for the vertical flow $H'p$, where $H' = \frac{K'}{b'T}$. K' and b' are the vertical hydraulic conductivity and the thickness of the overlaying aquifer respectively. T is the transmissivity of the target aquifer.

$$\frac{\partial^2 p}{\partial r^2} + \frac{1}{r}\frac{\partial p}{\partial r} - H'p = \frac{\phi\mu c_t}{k}\left(\frac{\partial p}{\partial t} - B\frac{\partial \sigma_t}{\partial t}\right) \tag{28}$$

The inner boundary conditions with skin effect and wellbore storage are given by Equations 6 and 7. The outer boundary condition at $r = \infty$, however, is not $B\sigma_t$ any more due to the influence of the vertical flow. Instead, the outer boundary follows a cyclic function $p_\infty(t)$ with the same frequency as σ_t but a different amplitude $p_{\infty 0}(\omega)$:

$$p_\infty(t) = p_{\infty 0}(\omega)\exp(i\omega t) \tag{29}$$

The relationship between $p_{\infty 0}$ and σ_0 can be found by inserting Equations 13 and 29 into the governing Equation 28, which yields:

$$-H'p_{\infty 0} = \frac{i\omega\phi\mu c_t}{k}(p_{\infty 0} - B\sigma_0) \tag{30}$$

and $p_{\infty 0}$ is given as:

$$p_{\infty 0} = \frac{i\omega\phi\mu c_t/k}{i\omega\phi\mu c_t/k + H'}B\sigma_0 = \frac{\alpha_D^2}{\alpha_D^2 + H'_D}B\sigma_0 \tag{31}$$

where $H'_D = H'r_w^2$.

By defining:

$$p'(r,t) = p(r,t) - p_\infty(t) \tag{32}$$

and using Equation 30, the governing equation in terms of p' is obtained as:

$$\frac{\partial^2 p'}{\partial r^2} + \frac{1}{r}\frac{\partial p'}{\partial r} - H'p' = \frac{\phi\mu c_t}{k}\frac{\partial p'}{\partial t} \tag{33}$$

with the homogeneous outer boundary condition:

$$p'(\infty,t) = 0 \tag{34}$$

Since $p'(r,t)$ is also a cyclic function, we can assume:

$$p'(r,t) = p'_0(r,\omega)\exp(i\omega t) \tag{35}$$

and p_w is given by Equation 15. Then Equation 33 becomes an ordinary differential equation in terms of $p'_0(r,\omega)$:

$$\frac{d^2p'_0}{dr^2} + \frac{1}{r}\frac{dp'_0}{dr} - H'p'_0 = \frac{i\omega\phi\mu c_t}{k}p'_0 \tag{36}$$

with the following boundary conditions:

$$p'_0(\infty,\omega) = 0 \tag{37}$$

$$p_{w0} = \left[p'_0 - s\left(r\frac{\partial p'_0}{\partial r}\right)\right]_{r=r_w} + p_{\infty 0} \tag{38}$$

$$i\omega C p_{w0} = \frac{2\pi kh}{\mu}\left(r\frac{\partial p'_0}{\partial r}\right)_{r=r_w} \tag{39}$$

The solution to Equation 36 considering the outer boundary condition, Equation 37, is:

$$p'_0(r,\omega) = A_3 K_0\left(r\sqrt{H' + \frac{i\omega\phi\mu c_t}{k}}\right) \tag{40}$$

From the boundary condition, Equation 39, we have:

$$\begin{aligned} A_3 &= -\frac{i\omega\mu C}{2\pi khr_w\sqrt{H' + i\omega\phi\mu c_t/k}K_1(r_w\sqrt{H' + i\omega\phi\mu c_t/k})}p_{w0} \\ &= -\frac{\alpha_D^2}{2S_D\beta_D K_1(\beta_D)}p_{w0} \end{aligned} \tag{41}$$

where β_D is defined as:

$$\beta_D = r_w\sqrt{H' + \frac{i\omega\phi\mu c_t}{k}} = \sqrt{H'_D + \alpha_D^2} \tag{42}$$

From the inner boundary condition, Equation 38, p_{w0} is obtained as:

$$p_{w0} = \left[1 + \frac{\alpha_D^2}{2S_D\beta_D}\frac{K_0(\beta_D)}{K_1(\beta_D)} + \pi i\frac{s}{T_D}\right]^{-1} p_{\infty 0} \tag{43}$$

Using Equation 31, we can express p_{w0} as:

$$p_{w0} = \left[1 + \frac{\alpha_D^2}{2S_D\beta_D}\frac{K_0(\beta_D)}{K_1(\beta_D)} + \pi i\frac{s}{T_D}\right]^{-1}\left(\frac{\alpha_D}{\beta_D}\right)^2 B\sigma_0 \tag{44}$$

With the solution, Equation 44, we can evaluate the wellbore storage coefficient and skin factor in a leaky aquifer using tidal analysis if properties of the overlaying permeable aquitard are available. It is also feasible to estimate the magnitude of the vertical leakage with different levels of wellbore storage effects and skin effects. Applications of the solution as well as the comparison between the confined aquifer solution and the semiconfined aquifer solution are explained in detail in Section 3.

3 Application

As explained in the introduction section (Section 1), two key parameters produced by tidal analysis are the amplitude ratio and the phase difference. The amplitude ratio is the ratio of the amplitude of a tidal constituent from the data to that of the same constituent from the theoretical tide (i.e. the loading efficiency). Similarly, the phase difference refers to the difference between the phase of a tidal constituent from the data to that from the theoretical tide. It is elucidated in this section how the amplitude ratio and the phase difference are related to aquifer and wellbore properties, based on the solutions derived in Section 2. Specifically, the influences of wellbore storage and skin effects are discussed in detail for both confined aquifer and semiconfined aquifer. The results for confined aquifer and semiconfined aquifer are compared to illustrate the effects of vertical leakage with different skin factors.

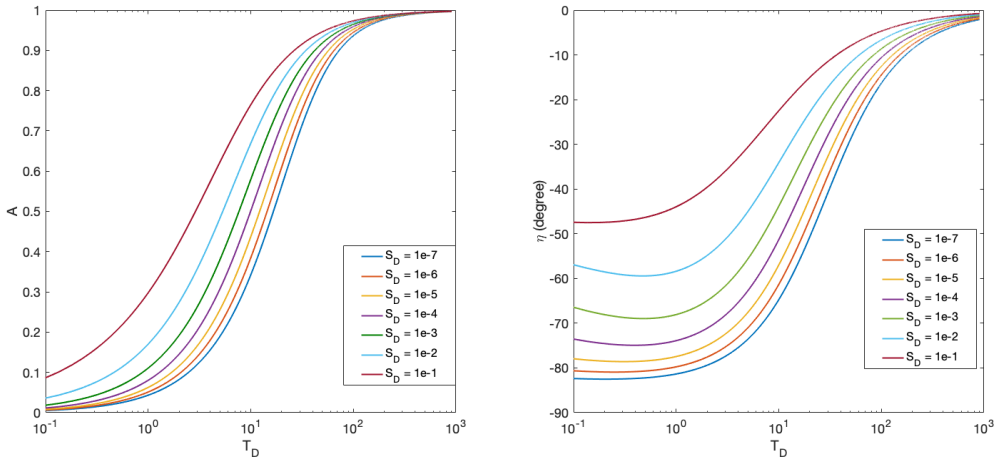

(a) A vs T_D for different S_D (b) η vs T_D for different S_D

Figure 3. (a) Amplitude ratio A and (b) phase shift η as a function of T_D for different S_D when skin is zero

3.1 Confined aquifer

On the basis of the solution for confined aquifers given by Equation 27, the amplitude ratio A and phase difference η can be expressed in terms of S_D, T_D and the skin factor s.

$$A = |p_{w0}/B\sigma_0| = \left| \left[1 + \frac{\alpha_D}{2S_D} \frac{K_0(\alpha_D)}{K_1(\alpha_D)} + \pi i \frac{s}{T_D} \right]^{-1} \right| \tag{45}$$

$$\eta = \arg(p_{w0}/B\sigma_0) = \arg\left(\left[1 + \frac{\alpha_D}{2S_D} \frac{K_0(\alpha_D)}{K_1(\alpha_D)} + \pi i \frac{s}{T_D} \right]^{-1} \right) \tag{46}$$

where $|z|$ and $\arg(z)$ are the modulus and the argument of the complex number z, respectively (Sato, 2015). A is the ratio of amplitude of wellbore pressure fluctuation p_{w0} to the theoretical tidal fluctuation $B\sigma_0$, which is also the outer boundary condition. The phase shift η is the difference in phase angles of p_{w0} and σ_0. When the wellbore pressure response lags behind the tidal stress disturbance, η becomes negative. In contrast, positive phase shift (phase advance) indicates wellbore pressure response leads the tidal stress.

For fixed values of skin factor and S_D, the amplitude ratio A and the phase shift η can be plotted as a function of T_D, as shown in Figure 3 when the skin factor is set to zero. Note that when the skin effect does not exist (i.e. skin factor is zero), the profiles of A and η shown in Figure 3 are exactly the same as those in the paper by Hsieh et al. (1987).

When the skin factor is nonzero, however, the profiles of A and η deviate from those when s is zero. Figure 4 a and b show A and η, respectively, as a function of T_D for different values of s and $S_D = 10^{-7}$. Figure 5 and 6 show the same plots as Figure 4 but with different S_D values ($S_D = 10^{-4}$ for Figure 5, and $S_D = 10^{-1}$ for Figure 6). It can be seen from Figure 4 that when S_D is relatively small (i.e. dimensionless wellbore storage coefficient is relatively large), the amplitude ratio becomes smaller and the phase shift becomes more negative as the skin factor increases from -5 to 30. This observation makes physical sense because larger skin factor indicates lower permeability around the wellbore and greater difficulty for aquifer fluid to flow into and out of the wellbore, resulting in smaller amplitude ratio and wider phase lag. However, this is only true when the wellbore storage effect is significant and dominates the behavior of pressure fluctuations in response to tidal forces. On the

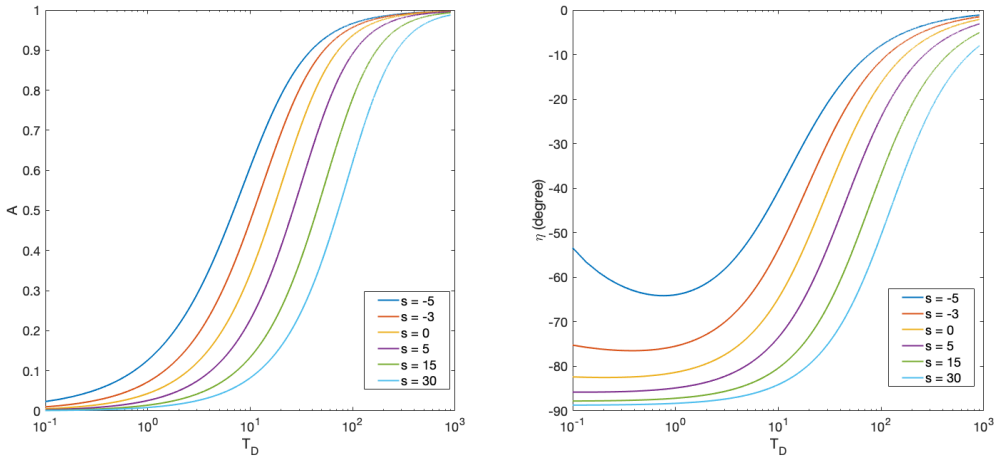

(a) A vs T_D for different s (b) η vs T_D for different s

Figure 4. (a)Amplitude ratio A and (b) phase shift η as a function of T_D for different skin s when $S_D = 10^{-7}$

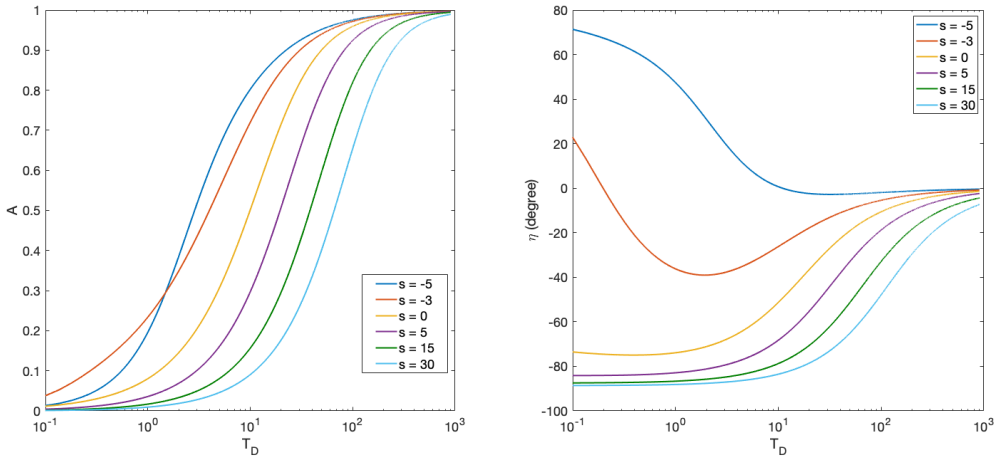

(a) A vs T_D for different s (b) η vs T_D for different s

Figure 5. (a)Amplitude ratio A and (b) phase shift η as a function of T_D for different skin s when $S_D = 10^{-4}$

other hand, when the wellbore storage effect is insignificant (S_D is relatively large) and when aquifer transmissivity is small, the effect of superposition caused by nonzero skin factor becomes more dominant. As discussed by Gieske and De Vries (1985) and Maas and De Lange (1987), negative phase shift or phase advance can appear in a composite aquifer when the inner zone is more permeable than the outer zone, as explained by the principle of superposition. Negative skin means the permeability of the inner zone (i.e. the damaged zone) is larger than that of the outer zone, so phase lag can be narrowed or even turn to phase advance when the skin is negative.

In Figure 5, S_D is 10^{-4}, which is in between 10^{-7} and 10^{-1}, so both the wellbore storage effect and the superposition effect influence the pressure response. As a result, the value of dimensionless transmissivity T_D becomes more important. When T_D is relatively

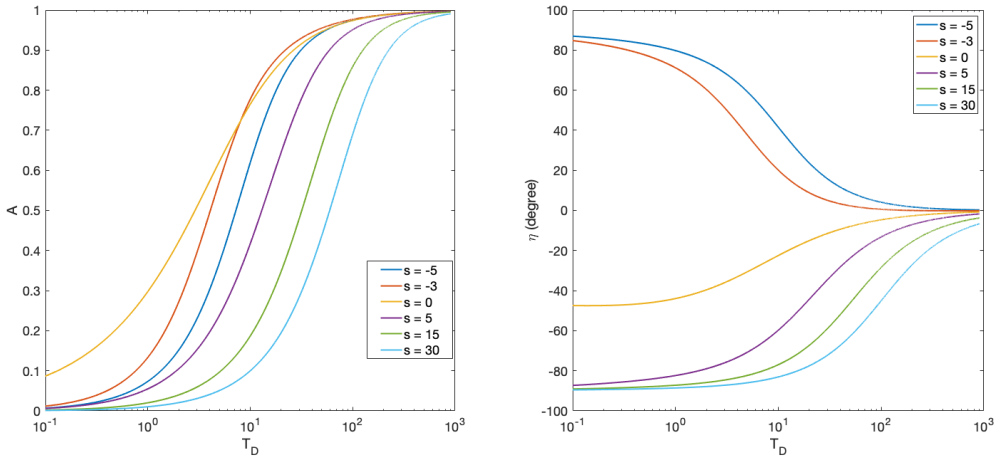

(a) A vs T_D for different s (b) η vs T_D for different s

Figure 6. (a)Amplitude ratio A and (b) phase shift η as a function of T_D for different skin s when $S_D = 10^{-1}$

Table 2. Dominant effect with various T_D and S_D values in confined aquifer

	small S_D	medium S_D	large S_D
small T_D	wellbore storage effect dominate	superposition effect dominate	superposition effect dominate
large T_D		wellbore storage effect dominate	

large, the wellbore storage effect plays a more significant role, while the superposition effect is more dominant when T_D is relatively small. As a result, when T_D is large, increasing skin from -5 to 30 decreases the amplitude ratio and increases the magnitude of the phase lag, which is the same as the observation in Figure 4. When T_D is small, however, the conclusion depends on the sign of the skin factor, and a positive skin results in a decrease in the amplitude ratio and an increase in the phase lag, while a negative skin manifests the opposite effects in A and η. When S_D is large, as is the case in Figure 6, the wellbore storage effect is weaker than the superposition effect regardless of the level of T_D, so the observation is the same with that from Figure 5 when T_D is relatively small, i.e. a more negative skin is associated with larger phase advance and smaller amplitude ratio while a more positive skin results in larger phase lag and smaller amplitude ratio. The observed trends are summarized in Table 2 and Table 3.

3.2 Semiconfined aquifer

The amplitude ratio A and phase shift η for semiconfined aquifers can be derived from the solution, Equation 44:

$$A = |p_{w0}/B\sigma_0| = \left| \left[1 + \frac{\alpha_D^2}{2S_D\beta_D} \frac{K_0(\beta_D)}{K_1(\beta_D)} + \pi i \frac{s}{T_D} \right]^{-1} \left(\frac{\alpha_D}{\beta_D} \right)^2 \right| \tag{47}$$

$$\eta = \arg(p_{w0}/B\sigma_0) = \arg\left(\left[1 + \frac{\alpha_D^2}{2S_D\beta_D} \frac{K_0(\beta_D)}{K_1(\beta_D)} + \pi i \frac{s}{T_D} \right]^{-1} \left(\frac{\alpha_D}{\beta_D} \right)^2 \right) \tag{48}$$

Table 3. Effect of skin on A and η under different scenarios

	wellbore storage effect dominant	superposition effect dominant
negative skin	A decreases and η becomes more negative (larger phase lag) when s increases from a negative value to zero.	A decreases and η becomes more positive (larger phase advance) when s decreases from zero to a negative value
positive skin	A decreases and η becomes more negative (larger phase lag) when s increases from zero to a positive value	

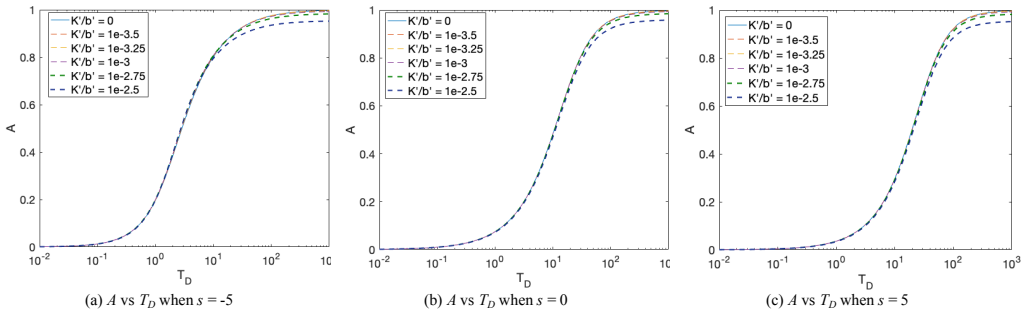

(a) A vs T_D when s = -5 (b) A vs T_D when $s = 0$ (c) A vs T_D when $s = 5$

Figure 7. Amplitude ratio A vs. T_D for various K'/b' when (a) $s = -5$, (b) $s = 0$ and (c) $s = 5$. The unit of K'/b' is s^{-1}.

We can see from Equations 47 and 48 that for a semiconfined aquifer A and η are determined by not only T_D and S_D but also by H', and H' reflects the magnitude of the vertical leakage ($H' = \frac{K'}{b'T}$).

Note that based on Equation 24, T_D is affected by both the tidal frequency ω and the aquifer permeability k. Therefore, when plotting A or η against T_D, we can change T_D through changing ω or k. For a confined aquifer, whether changing ω or k to change T_D does not influence the results, because A and η are functions of S_D and T_D only. For a semiconfined aquifer, however, the results will be different, because ω affects only T_D but k affects both T_D and H'. Thus, the profiles of A and η for semiconfined aquifer are discussed under two conditions. In the first condition, T_D varies with changing k, while in the second condition T_D varies with changing ω. Note that in practice, ω can only take discrete values (e.g. diurnal or semidiurnal) instead of continuous values, so the purpose of plotting A and η against T_D by varying ω is only to see the trends of the profiles of A and η when ω takes different values. For the following discussion in this section, S_D is set to be 10^{-4}.

Figures 7 a, b, and c show the effect of K'/b' on A for $s = -5$, $s = 0$, and $s = 5$ respectively under the first condition where T_D varies with k. K' and b' are the vertical hydraulic conductivity and the thickness of the overlaying aquifer respectively. In Figure 7 and 8, the unit of K'/b' is s^{-1}. It can be seen from Figure 7 that A tends to decrease with increasing K'/b', which makes physical sense because the amplitude of the pressure response measured at the wellbore is less sensitive to the tidal stress with greater vertical leakage. When K'/b' reduces, the profile of A converges to that from the confined aquifer solution. In addition, when s increases from -5 to 5, the curve moves from the left to the right, which is the same as our observation from Figure 4a, so in this case increasing the skin factor decreases A for fixed T_D.

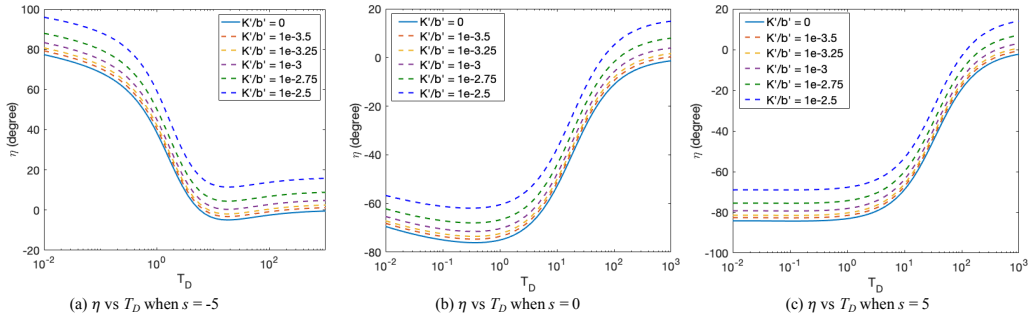

(a) η vs T_D when s = -5 (b) η vs T_D when s = 0 (c) η vs T_D when s = 5

Figure 8. Phase shift η vs. T_D for various K'/b' when (a) $s = -5$, (b) $s = 0$ and (c) $s = 5$. The unit of K'/b' is s^{-1}.

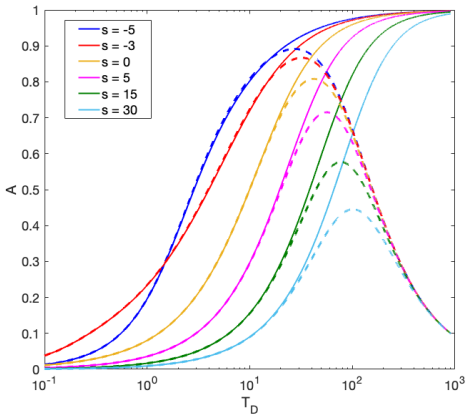

Figure 9. Amplitude ratio A vs. T_D for different skin factor

The profiles of η with various K'/b' for $s = -5$, $s = 0$ and $s = 5$ are shown in Figures 8 a, b and c respectively under the first condition where T_D varies with k. In Figure 8, when s is negative, the phase advance becomes larger with increasing K'/b' (greater vertical leakage). When s is zero or positive, the phase lag reduces and becomes less negative with increasing K'/b'. Thus, greater vertical leakage causes η to change in the same upward direction regardless of the sign of the skin factor. Furthermore, with our solution, the effects of vertical leakage can be separated from the effects of enhanced horizontal permeability, making it feasible to evaluate skin factor from tidal analysis even in the presence of vertical flow. For example, when $s = -5$ and $T_D = 2.854$, the phase advance caused solely by negative skin with $K'/b' = 0$ is 12.05°. When $K'/b' = 10^{-3}$, the total phase advance increases to 17.71°, and vertical leakage accounts for 32% of the phase advance. When K'/b' further increases to $10^{-2.5}$, the total phase advance becomes 30.1°, 60% of which is due to vertical leakage.

Under the second condition, T_D varies with ω and k is kept constant. When K'/b' is 10^{-5}, which is relatively small in this case, the profile of A is almost the same as that shown in Figure 4a. When K'/b' increases to 10^{-3}, however, the curves become bell-shaped. In Figure 9, the solid curves and dashed curves represent results for confined aquifer and semiconfined aquifer respectively, and each color represents a skin factor value. It can be seen from Figure 9 that the difference between A for confined aquifer and A for semiconfined aquifer increases with T_D. At larger T_D, the amplitude ratio for a semiconfined aquifer is lower than that for a confined aquifer. The profiles of η under the second condition are

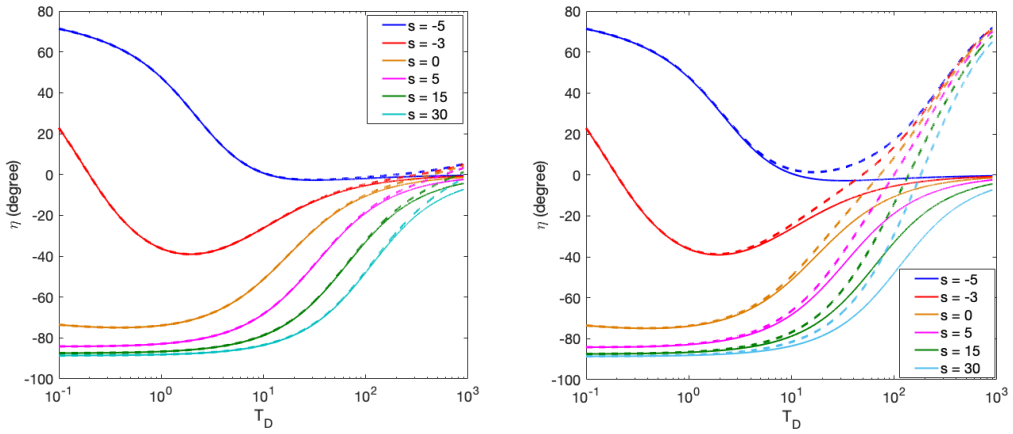

(a) $K'/b' = 10^{-5}$ (b) $K'/b' = 10^{-3}$

Figure 10. Phase shift η vs. T_D for different skin factor when (a) $K'/b' = 10^{-5}$ and (b) $K'/b' = 10^{-3}$

shown in Figure 10. Similarly, when K'/b' is relatively small, η for a semiconfined aquifer is very close to that for a confined aquifer, but when K'/b' rises up, the difference is enlarged, especially when T_D is large. The phase shift is larger (less negative or more positive) with vertical flow. One possible explanation for the observation that A and η for the semiconfined aquifer are more different than those for the confined aquifer when T_D is larger is that the effect of vertical leakage is more dominant for larger T_D, while the permeability change due to the skin effect plays a more significant role when T_D is smaller.

In general, vertical leakage tends to decrease the amplitude ratio and increase the phase advance or decrease the phase lag. The effects of vertical flow and the effects of skin can be quantified separately, so we can still infer the skin factor using tidal analysis even in a semiconfined aquifer.

4 Examples

4.1 Example for confined aquifer

In previous studies, tidal analysis was applied to estimate transmissivity or permeability of confined aquifers, which provides a cost-effective monitoring approach (Hsieh et al., 1987; Elkhoury et al., 2006; Allègre et al., 2016; Narasimhan et al., 1984). The skin effect, however, was not considered in these studies. Our theoretical solution indicates that the skin effect has a significant impact on the interpretation of the phase difference obtained from tidal analysis and the estimation of aquifer transmissivity. In this section, a case study originally discussed by Hsieh et al. (1987) is reanalyzed to illustrate the potential impact of the skin effect on the estimation of aquifer transmissivity. In the paper by Hsieh et al. (1987), water level data measured during February 24 to June 23 in 1985 from an open well at a site about 11 km from Parkfield, California (the Gold Hill site) were analyzed and compared to the dilatation record collected by dilatometers installed at the same site to obtain the phase difference corresponding to the M_2 tidal component. Key wellbore and aquifer parameters used for the analysis are listed in Table 4. More details about the data and the geological background can be found in the paper by Hsieh et al. (1987).

Table 4. Wellbore and aquifer properties for the confined aquifer example (Hsieh et al., 1987)

parameter	value/range
well depth	88 m
well casing depth	18.3 m
casing radius	7.0 cm
open-hole radius	7.0 cm
storativity S	$10^{-6} \sim 10^{-4}$

In the paper by Hsieh et al. (1987), the smoothed water fluctuation data and dilatation data were analyzed with the Fourier transform to compute the phase shift of M_2 tidal constituent, which is the dominant tidal constituent. In this case, the mean M_2 phase shift was found to be -11.6°. Based on the mean M_2 phase shift and the range of storativity S $(10^{-6} - 10^{-4})$, assuming the skin factor is zero, Hsieh et al. (1987) estimated the range of aquifer transmissivity to be around $8 \times 10^{-6} - 2 \times 10^{-5}$ m^2/s. Hsieh et al. (1987) did not mention if the skin effect was present at the studied well, so our discussion here is around the question of how the estimation of aquifer transmissivity would change if the skin effect had existed in this case. In this study, it is found that with the same input parameters, nonzero skin factor can result in a significantly different estimation of aquifer transmissivity.

In Figure 11, the solid blue curve and the solid red curve represent the relation between the aquifer transmissivity T and the phase difference η when skin is assumed to be zero, and the dashed curves indicate nonzero skin factors and are based on the solutions proposed in this study. The estimated range of T given the range of S $(10^{-6} - 10^{-4})$ can be found by measuring the space between the blue curves and the red curves. It can be seen from Figure 11 that positive skin factors shift the curves to the right, and negative skin factors shift the curves to the left, which means the estimation of aquifer transmissivity should increase with positive skin factor and decrease with negative skin factor. Figure 11b is a zoomed-in version of Figure 11a, and the estimated range of T can be better seen in Figure 11b when the M_2 phase difference is -11.6°, which is shown by the black horizontal line. In this case, a positive skin factor of 5 would change the estimated range of T to $2 \times 10^{-5} - 2.4 \times 10^{-5}$ m^2/s, and a negative skin factor of -3 would change the estimation to $3 \times 10^{-6} - 8 \times 10^{-6}$ m^2/s. If we compare the mean values of the estimated transmissivities, we can see that the estimation in aquifer transmissivity would increase by $\sim$57% if the skin factor is increased to 5 from 0 and decrease by $\sim$60% if the skin factor is decreased to -3 from 0, so the change in aquifer transmissivity estimation is significant when the skin effect is included.

Through this example, it is demonstrated that the consideration of skin effect is important in tidal analysis, and the solution proposed in this study should be applied to give an accurate transmissivity estimation when the wellbore is damaged or stimulated, which occurs frequently in practice.

4.2 Example for semiconfined aquifer

For semiconfined aquifers, factors influencing the phase difference between the tidal signal and the theoretical tide include aquifer transmissivity, wellbore storage, skin factor, and the level of vertical leakage. If three out of these four factors and the phase difference are known, the remaining one factor can be assessed using our solution for semiconfined aquifer illustrated in Section 2.3. If the skin effect exists but is neglected (i.e. s is assumed to be 0), only three factors are left in the consideration, and then the assessment of one of the three factors based on the other two could be inaccurate. Wang et al. (2018) applied the semiconfined aquifer model to the evaluation of vertical leakage using tidal analysis, without discussing whether the skin effect existed at the well where the tidal response were

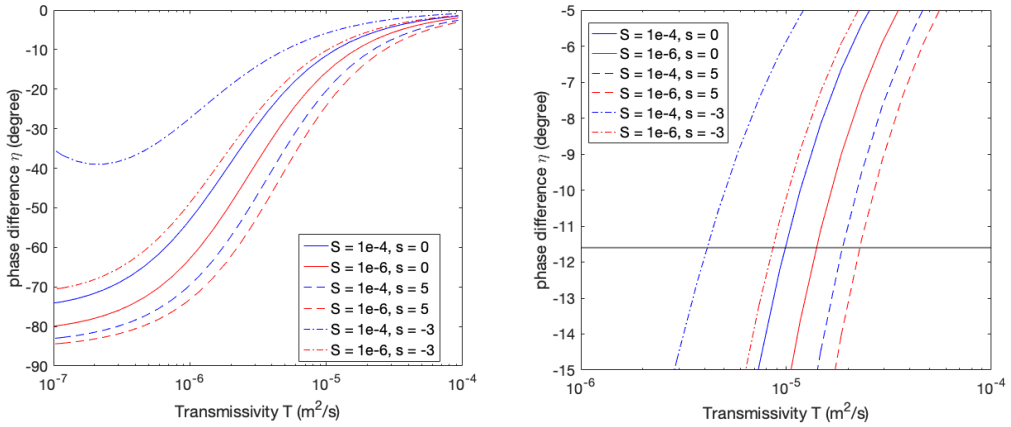

(a) Phase difference vs. T

(b) Phase difference vs. T zoomed part

Figure 11. Change in transmissivity estimation due to the skin effect

Table 5. Wellbore and aquifer properties for the semiconfined aquifer example (Wang et al., 2018)

parameter	value/range
well depth	960 m
wellbore radius	11 cm
casing radius	3.65 cm
aquifer transmissivity T	$9.6 \times 10^{-6} - 1.4 \times 10^{-3}$ m^2/s
storativity S	$2.6 \times 10^{-6} - 2.7 \times 10^{-5}$

collected. If the well in the paper by Wang et al. (2018) was not damaged nor stimulated ($s = 0$), then the original evaluation of vertical leakage proposed by Wang et al. should be accurate. If the skin factor was nonzero, however, the evaluation of vertical leakage could alter. Our discussion here focuses on the extent to which the evaluation of vertical leakage could change if the skin factor was nonzero.

Data used by Wang et al. (2018) were collected from a deep monitoring well in the Arbuckle aquifer in Oklahoma by the U.S. Geological Survey (USGS) starting from April, 2017. The data and the well information are available on USGS website (`https://waterdata.usgs.gov/nwis/uv/?site\_no=364337096315401`). It is believed that there is a leaky aquitard overlaying the target aquifer, and the bottom of the target aquifer is confined by an impermeable layer. Table 5 lists some key well and aquifer parameters required for the analysis. More details about the site and the data are available in the paper by Wang et al. (2018) and the USGS website.

Wang et al. (2018) found that the water level tidal response leads the theoretical tide, and the phase advance is estimated to be 12.5°. Based on the range of transmissivity and storativity in Table 5, the range of specific leakage K'/b' (i.e. the ratio of the vertical hydraulic conductivity of the leaky aquitard to the thickness of the aquitard), was estimated to be $10^{-10} - 10^{-9}$ s^{-1} if the skin factor was zero.

Based on our analytical solution and the illustration in Section 3, we know that the effect of skin factor on the amplitude ration A and the phase difference η is tapered when transmissivity is relatively large. For instance, in Figure 9 and Figure 10, curves correspond-

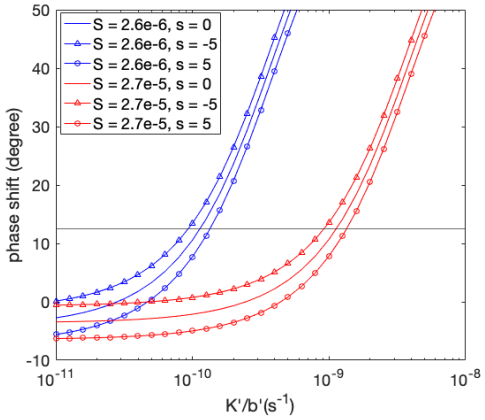

Figure 12. Change in vertical leakage estimation due to the skin effect

ing to different skin factors converge as T_D becomes larger. Our finding in this example of a semiconfined aquifer coincides with this theoretical conclusion, because when the aquifer transmissivity is as large as 1.4×10^{-3} m^2/s (the upper bound of transmissivity provided by Wang et al. (2018), see Table 5), various skin factors result in similar estimation of K'/b' (i.e. $10^{-10} - 10^{-9}$ s^{-1}). When transmissivity is 9.6×10^{-6} m^2/s, however, the range of K'/b' deviates from the original estimation depending on the value of skin factor. Figure 12 shows the change in K'/b' estimation due to the skin effect when $T = 9.6 \times 10^{-6}$ m^2/s. The solid lines represent the cases when skin factor is zero, and the space between the red curve and the blue curve indicates the estimated range of K'/b'. Results when $s = -5$ and $s = 5$ are shown by the dash-dot lines and the dashed lines respectively. It can be seen from Figure 12 that when $s = -5$, the estimated range of K'/b' reduces to $9.2 \times 10^{-11} - 9.1 \times 10^{-10}$ m^2/s, and when $s = 5$, the range increases to $1.5 \times 10^{-10} - 1.4 \times 10^{-9}$ m^2/s.

Positive skin factor increases the estimation, because with a larger skin factor, it requires a higher level of vertical leakage to reach the same phase advance. Similarly, negative skin factor reduces the estimated range of vertical leakage. The skin effect should be taken into consideration when evaluating the level of vertical leakage in a semiconfined aquifer from tidal analysis, especially when the aquifer transmissivity is not very large.

5 Summary

Our work can be summarized as follows.

1. The effects of Earth tide on aquifers are modeled theoretically with wellbore storage effects and skin effects taken into consideration. Models are developed for both confined aquifers and semiconfined aquifers.
2. For confined aquifers, amplitude ratio and phase shift are determined by aquifer transmissivity, wellbore storage, and the skin factor. It is found that higher positive skin factor can lead to larger phase lag due to greater difficulty for aquifer fluid to flow into and out of the wellbore. In addition, the phase shift in a confined aquifer is not always negative - a phase advance can occur when the skin factor is negative with enhanced permeability around the wellbore, and the phase advance with more negative skin is larger.
3. In practice the target aquifer is sometimes not perfectly confined (semiconfined), and there exists vertical leakage in semiconfined aquifers. In semiconfined aquifers, the magnitude of the vertical leakage also affects the amplitude ratio and phase shift

besides transmissivity, wellbore storage and skin factor. Our solution for semiconfined aquifers indicates that greater vertical leakage tends to result in smaller amplitude ratio and larger phase advance or smaller phase lag. The effect of vertical leakage is stronger when aquifer permeability is higher and/or tidal frequency is lower. Based on our solution, we can separate the effect of vertical leakage and the effect of enhanced permeability in semiconfined aquifers and evaluate the phase shift contributed by each of the two effects independently.

4. Real-world examples based on previous work by Hsieh et al. (1987) and Wang et al. (2018) are analyzed to demonstrate the effects of nonzero skin factors on transmissivity estimation for confined aquifers and vertical leakage estimation for semiconfined aquifers. It is found that the skin effect has significant influence on the final results from tidal analysis and should be included in tidal response models.

Appendix A Solving the governing equation with Laplace transform

The governing partial differential equations discussed in Section 2 can be solved with Laplace transform. The dimensionless form of the governing equation for confined aquifer (Equation 4) is:

$$\frac{\partial^2 p_D}{\partial r_D^2} + \frac{1}{r_D}\frac{\partial p_D}{\partial r_D} = \frac{\partial p_D}{\partial t_D} - B\frac{d\sigma_D}{dt_D} \tag{A1}$$

The dimensionless forms are:

$$p_D = \frac{2\pi kh}{q\mu}(p_i - p) \tag{A2}$$

$$t_D = \frac{kt}{\phi\mu c_t r_w^2} \tag{A3}$$

$$r_D = r/r_w \tag{A4}$$

$$\sigma_D = \frac{2\pi kh}{q\mu}\sigma \tag{A5}$$

where p_i is the initial aquifer pressure, and the rest of the variable are the same as those previously defined in Section 2. The dimensionless boundary conditions are:

$$p_D(\infty, t_D) = B\sigma_D(t_D) \tag{A6}$$

$$p_{wD} = \left[p_D - s\left(r_D\frac{\partial p_D}{\partial r_D}\right)\right]_{r_D=1} \tag{A7}$$

$$C_D\frac{\partial p_{wD}}{\partial t_D} - \left(r_D\frac{\partial p_D}{\partial r_D}\right)_{r_D=1} = 1 \tag{A8}$$

Define $y_D = p_D - B\sigma_D$, then the system of equations become:

$$\frac{\partial^2 y_D}{\partial r_D^2} + \frac{1}{r_D}\frac{\partial y_D}{\partial r_D} = \frac{\partial y_D}{\partial t_D} \tag{A9}$$

$$y_D(\infty, t_D) = 0 \tag{A10}$$

$$p_{wD} = \left[y_D - s\left(r_D\frac{\partial y_D}{\partial r_D}\right)\right]_{r_D=1} + B\sigma_D(t_D) \tag{A11}$$

$$C_D\frac{\partial p_{wD}}{\partial t_D} - \left(r_D\frac{\partial y_D}{\partial r_D}\right)_{r_D=1} = 1 \tag{A12}$$

The governing equation in the Laplace space can be obtained by applying the Laplace transform to Equation A9.

$$\lambda\overline{y_D} = \frac{1}{r_D}\frac{\partial}{\partial r_D}\left(r_D\frac{\partial\overline{y_D}}{\partial r_D}\right) \tag{A13}$$

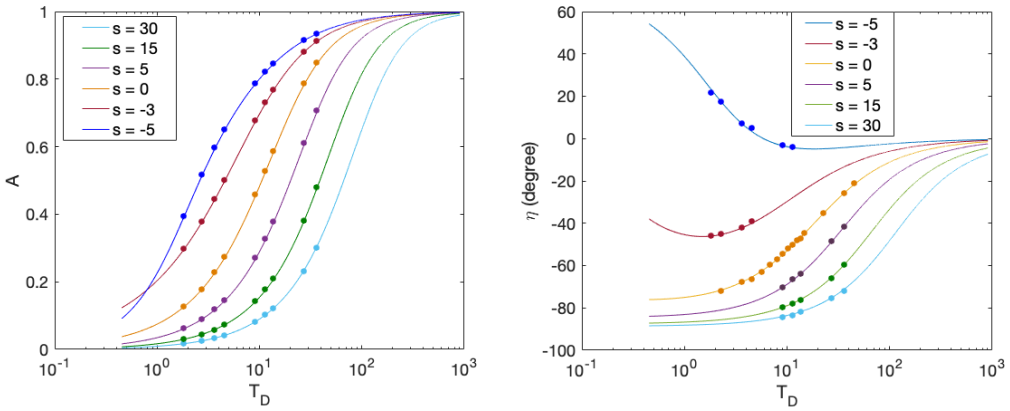

(a) A vs T_D for different s (b) η vs T_D for different s

Figure A1. Verification of the results with Laplace transform

where λ is the Laplace variable, and the overline indicates corresponding variables in the Laplace space. Note that Equation A13 is an ordinary differential equation, and the general solution considering boundary condition A10 is $\overline{y_D} = A_4 K_0(\sqrt{\lambda} r_D)$. A_4 is a function of λ only. The boundary conditions, Equations A11 and A12, give that:

$$A_4 = \frac{1 - C_D \lambda^2 B \overline{\sigma_D(\lambda)}}{C_D \lambda^2 (K_0(\sqrt{\lambda}) + s\sqrt{\lambda} K_1(\sqrt{\lambda})) + \lambda\sqrt{\lambda} K_1(\sqrt{\lambda})} \tag{A14}$$

The solution in the Laplace space is:

$$\overline{p_{wD}} = \frac{K_0(\sqrt{\lambda}) + \sqrt{\lambda} K_1(\sqrt{\lambda})(s + \lambda B \overline{\sigma_D})}{C_D \lambda^2 (K_0(\sqrt{\lambda}) + s\sqrt{\lambda} K_1(\sqrt{\lambda})) + \lambda\sqrt{\lambda} K_1(\sqrt{\lambda})} \tag{A15}$$

Equation A15 is the general solution when the flow rate is nonzero. When the flow rate is zero, however, we cannot transform the variables into the dimensionless form and need to solve the system of equations in its dimensional form using the Laplace transform, which process is the same as the steps illustrated in this appendix. The solution for closed well in the dimensional form is:

$$\begin{aligned} \overline{p_w} &= \frac{\lambda\sqrt{\lambda} K_1(\sqrt{\lambda}) B \overline{\sigma}}{C_D \lambda^2 (K_0(\sqrt{\lambda}) + s\sqrt{\lambda} K_1(\sqrt{\lambda})) + \lambda\sqrt{\lambda} K_1(\sqrt{\lambda})} \\ &= \left[1 + \frac{C_D \sqrt{\lambda} K_0(\sqrt{\lambda})}{K_1(\sqrt{\lambda})} + s C_D \lambda\right]^{-1} B \overline{\sigma} \end{aligned} \tag{A16}$$

Equation A16 can be inverted numerically to attain the profiles of A and η. The numerical inversion is based on the method introduced by Talbot (1979). In Figure A1, the dots represent results from numerical inversion of the Laplace transform, and the solid lines represent results from Section 2. It can be seen that the Laplace transform gives results consistent with those from Section 2, thus verifying our solution.

Acknowledgments

This research is supported by the Stanford University Industrial Affiliates Program on Analysis of Earth Tides (SUPRI-Tides). The paper is theoretical, and data were not used, nor created for this research.

References

Allègre, V., Brodsky, E. E., Xue, L., Nale, S. M., Parker, B. L., & Cherry, J. A. (2016). Using earth-tide induced water pressure changes to measure in situ permeability: A comparison with long-term pumping tests. *Water Resources Research*, *52*(4), 3113–3126.

Arditty, P. C., Ramey Jr, H. J., & Nur, A. M. (1978). Response of a closed well-reservoir system to stress induced by earth tides. In *Spe annual fall technical conference and exhibition.*

Bartels, J. (1957). Tidal forces. *Gezeitenkräfte in Encyclopedia of Physics, S. Flügge Ed.*, *48*, 734–774.

Bredehoeft, J. D. (1967). Response of well-aquifer systems to earth tides. *Journal of Geophysical Research*, *72*(12), 3075–3087.

Burbey, T. J. (2010). Fracture characterization using earth tide analysis. *Journal of hydrology*, *380*(3-4), 237–246.

Cartwright, D., & Eden, A. (1973). Corrected table of tidal harmonics, geophys. *JR Astron. Soc*.

Cartwright, D. E., & Tayler, R. J. (1971). New computations of the tide-generating potential. *Geophysical Journal International*, *23*(1), 45–73.

Cinco-Ley, H., & Samaniego, V. (1977). Effect of wellbore storage and damage on the transient pressure behavior of vertically fractured wells. In *Spe annual fall technical conference and exhibition.*

Cooper, H. H., Bredehoeft, J. D., & Papadopulos, I. S. (1967). Response of a finite-diameter well to an instantaneous charge of water. *Water Resources Research*, *3*(1), 263–269.

Elkhoury, J. E., Brodsky, E. E., & Agnew, D. C. (2006). Seismic waves increase permeability. *Nature*, *441*(7097), 1135.

Gieske, A., & De Vries, J. J. (1985). An analysis of earth-tide-induced groundwater flow in eastern botswana. *Journal of Hydrology*, *82*(3-4), 211–232.

Gringarten, A. C., Bourdet, D. P., Landel, P. A., & Kniazeff, V. J. (1979). A comparison between different skin and wellbore storage type-curves for early-time transient analysis. In *Spe annual technical conference and exhibition.*

Hantush, M. S., & Jacob, C. E. (1955). Non-steady green's functions for an infinite strip of leaky aquifer. *Eos, Transactions American Geophysical Union*, *36*(1), 101–112.

Hicks, S. D., & Szabados, M. W. (2006). *Understanding tides.* US Department of Commerce, National Oceanic and Atmospheric Administration, National Ocean Service.

Hsieh, P. A., Bredehoeft, J. D., & Farr, J. M. (1987). Determination of aquifer transmissivity from earth tide analysis. *Water resources research*, *23*(10), 1824–1832.

Maas, C., & De Lange, W. J. (1987). On the negative phase shift of groundwater tides near shallow tidal rivers—the gouderak anomaly. *Journal of Hydrology*, *92*(3-4), 333–349.

Melchior, P. (1966). *The earth tides.* Oxford: Pergamon Press.

Melchior, P. (1983). The tides of the planet earth. *Organic Photonics and Photovoltaics*.

Narasimhan, T., Kanehiro, B., & Witherspoon, P. (1984). Interpretation of earth tide response of three deep, confined aquifers. *Journal of Geophysical Research: Solid Earth*, *89*(B3), 1913–1924.

Ramey Jr, H. J. (1970). Short-time well test data interpretation in the presence of skin effect and wellbore storage. *Journal of Petroleum Technology*, *22*(01), 97–104.

Sato, K. (2006). Monitoring the underground migration of sequestered carbon dioxide using earth tides. *Energy conversion and management*, *47*(15-16), 2414–2423.

Sato, K. (2015). *Complex analysis for practical engineering.* Springer.

Sato, K., & Horne, R. N. (2018). Time-lapse analysis of pressure transients due to ocean tides for estimating co2 saturation changes. *International Journal of Greenhouse Gas Control*, *78*, 160–167.

Schwiderski, E. W. (1980). On charting global ocean tides. *Reviews of Geophysics*, *18*(1), 243–268.

Talbot, A. (1979). The accurate numerical inversion of laplace transforms. *IMA Journal of Applied Mathematics*, *23*(1), 97–120.

Van der Kamp, G., & Gale, J. E. (1983). Theory of earth tide and barometric effects in porous formations with compressible grains. *Water Resources Research*, *19*(2), 538–544.

Wang, C.-Y., Doan, M.-L., Xue, L., & Barbour, A. J. (2018). Tidal response of groundwater in a leaky aquifer—application to oklahoma. *Water Resources Research*, *54*(10), 8019–8033.